Relation of Oil Yield to the Structure of the Thermal Wave in the Combustion Processing of Oil Shale

The combustion retorting of oil shale is analyzed. By using coordinate systems moving at the same velocity as reaction zones, a model is obtained for the fully developed thermal wave which would exist after the wave has progressed a sufficient distance into the bed. Of particular interest is the interpretation of oil yield in terms of the structure of the wave and of operating variables.

MILTIADIS HISKAKIS and T. J. HANRATTY

Department of Chemical Engineering
University of Illinois
Urbana, IL 61801

SCOPE

In the combustion retorting of oil shale, a combustion wave is caused to move down through a bed of raw shale particles. Hot gases flow ahead of the wave and decompose the kerogen in the raw shale. Oil produced by this pyrolysis reaction is carried from the hot zone as a vapor which condenses on cold shale particles and falls out the bottom of the bed as a liquid product. The pyrolysis of the kerogen leaves behind a carbon residue which provides the fuel for the combustion. The size of the oil yield from the process depends on keeping the combustion zone separated from the retorting zone and on minimizing the combustion of oil by oxygen which has bypassed the hot carbon residue.

We have been developing a simple model for this process in which we describe the characteristics of the wave after it moves a sufficient distance into the bed that the reaction zones have reached fully developed conditions. The flow is assumed to be uniform and adiabatic so that the wave is one-dimensional. By using a coordinate system moving at the same velocity as a reaction zone, the partial differential equations for the reaction zone become ordinary differential equations. The analysis is considerably simplified by neglecting dispersion of heat and mass in the flow direction and by assuming rock fragments small enough that no temperature gradients exist in the solid. Since the analysis uses separate equations for the solid and the gas, effects of heat dispersion can be taken into account by adjusting the heat transfer coefficient between the solid and gas (Hiskakis & Hanratty, 1983).

In the first of two related previous papers (Hiskakis and Hanratty, 1983) we presented results from an analysis of the combustion of a bed of particles impregnated with carbon. In the second paper (Hiskakis and Hanratty, 1985) the analysis is extended to particles containing carbonates and silicates; i.e., processed shale. In this paper we include the retorting of kerogen so that product yield can be related to process variables.

CONCLUSIONS AND SIGNIFICANCE

This paper presents the first calculations of the fully developed thermal wave for the combustion retorting of oil shale. A principle result of this paper is that the oil yield is related to the characteristics of the thermal waves already identified in the two previous papers. This physical understanding of the process allows us to propose an operating strategy.

The parameter β, defined in the first paper, emerges as being of critical importance. To our knowledge, all of the experimental retorts have operated under conditions that $\beta < 1$. We present a number of reasons why operation with $\beta > 1$ appears more advantageous.

INTRODUCTION

Oil shale is a sedimentary rock containing a small amount of high molecular weight organic material (kerogen) some carbonates, and a large amount of inert solid. The kerogen decomposes upon heating, into oil, gas, and a carbonaceous residue. If the heating occurs at a high enough temperature the carbonates decompose, releasing carbon dioxide.

In the combustion retorting of shale to produce oil, combustion of the carbonaceous residue supplies the heat for the pyrolysis. In this process the top of a rubblized bed of raw shale is ignited. A gas containing oxygen passes through the bed. It is heated to the combustion temperature when it contacts hot processed shale and burns the carbon left behind by the pyrolysis reaction. The gases from this combustion contact the raw shale, decomposing the carbonates and pyrolyzing the kerogen. The oil, which is carried from the hot zone as a vapor, condenses when it contacts cooler shale particles and falls out the bottom of the bed as a liquid product.

The thermal wave which moves through the bed consists of a number of zones: a thermal zone in which the raw shale is heated to the pyrolysis temperature, a zone in which the pyrolysis reaction occurs, a zone in which the carbonates decompose, a combustion zone, and a thermal zone in which the incoming gases are heated by the processed shale. In the operation of this process it is desirable to minimize the amount of oxygen bypassing the combustion zone so that it does not burn the oil produced.

This paper is the third in a series in which we describe the characteristics of the thermal wave after it has moved a sufficient distance into the bed to reach a fully developed condition. It emphasizes the influence of process conditions on yield. We assume the flow to be uniform and adiabatic and neglect the dispersion of heat and mass. We consider rock fragments small enough that temperature change inside the particles can be ignored. By using a coordinate system moving at the same velocity as a reaction zone the analysis is greatly simplified because the defining differential equations are ordinary, rather than partial.

In a previous paper (Hiskakis and Hanratty, 1983; hereafter HH-1) we studied the combustion of the carbonaceous residue remaining in a bed of shale that had been thermally processed to decompose all the kerogen and carbonates. We found a parameter, equal to the ratio of the heat capacity of the gas flow to the heat capacity of the solid flow,

$$\beta = \frac{\dot{m}_g C_g}{VA\rho_s C_s(1-\epsilon)}, \tag{1}$$

to be critically important in interpreting the combustion process.

For $\beta > 1$ the combustion occurs at the back part of the thermal wave, so that the combustion and solid heating zones are separated. The cold gas entering the retort can quench the combustion reaction, leaving a fraction of the carbon, ψ_s, unburned. The gas heating and combustion zones move slower than the solid heating zone so that the heat of combustion is stored in a region between the two zones that increases in size with increasing time.

For $\beta < 1$, the combustion occurs at the front end of the thermal wave, so that the combustion and solid heating zones are close together. In this case the combustion reaction can be quenched by contacting the cold unprocessed shale and a fraction of the incoming oxygen, η_s, will not be consumed. The combustion zone moves faster than the gas heating zone and, as is the case for $\beta > 1$, the heat of combustion is stored in a zone of increasing size between the combustion and solid heating zones.

For $\beta = 1$ the solid heating zone and the gas heating zone move at the same velocities. The heat of combustion is accommodated by an increasing temperature in the bed. This is obviously an unstable situation, which should be avoided.

In a second paper (Hiskakis and Hanratty, 1985; hereafter HH-2) we studied the combustion of a processed shale that contained both carbonaceous material and carbonates. The decomposition of the carbonates absorbs much of the heat of combustion so the bed does not reach as high a temperature as for the case considered in HH-1. The difference between the heat released by combustion and the heat absorbed by the endothermic reactions is represented by the dimensionless groups N_{di}. For example,

$$N_{d3} = T_{adc}/T_{di}, \tag{2}$$

where T_{adc} is the adiabatic reaction temperature for the case in which all the dolomite and calcite decompose, Eq. 15, and T_{di} is the temperature at which dolomite starts to decompose, Eq. 14. The case of $\beta > 1$, $N_{d3} > 1$ is of particular interest. For $N_{d3} > 1$ the heat released by the exothermic combustion is enough to decompose all the carbonates and cause the carbonate decomposition zone to move faster than the combustion zone. Since, also, $\beta > 1$, there is a separation between the combustion and the solid heating wave. Therefore, in this case ($\beta > 1$, $N_{d3} > 1$) a separation of the combustion, the carbonate decomposition, and the solid heating zones occurs.

In this paper we present the results of calculations in which we include the pyrolysis of the kerogen in addition to the combustion of carbon and the decomposition of carbonates. From our previous work, the case of $\beta > 1$, $N_{d3} > 1$ appeared particularly attractive because the combustion and the pyrolysis zones are the most separated and the fraction of the oxygen bypassing the combustion zone is zero. However, the case of $\beta < 1$ has the advantage of higher heating rates during the pyrolysis reaction than the case of $\beta > 1$. This means that yield losses by coking of the oil should be less severe for $\beta < 1$ since the oil produced will be vaporized very fast. Consequently, a question we are most interested in exploring is whether advantages of operating at conditions such that $\beta > 1$, $N_{d3} > 1$ are offset by troubles associated with coking.

The novelty of the calculations presented in this paper is that they focus on the thermal wave under a fully developed condition. This approach has the advantages of requiring smaller computer time and of more easily presenting the relationship of the structure of the thermal wave to the physical processes that are occurring. Previous calculations of fully developed temperature waves by Fausset (1975) and by Baer and Dahl (1980) are significant in that they point out the importance of parameter β, but have limitations already discussed in HH-1.

All of the models described in the literature for the combustion retorting (Braun, 1981; Tyner and Hommert, 1979; Nuttal, 1976; Ahmad et al., 1977) consider the thermal wave under transient conditions. Their agreement with experimental results obtained in retorts of limited length is quite good. However, their nonlinearity, as well as their complexity, makes these models time consuming. Furthermore, the limitations of the grid size imposed by time considerations and the numerical precision of the computation can cause numerical instabilities. In some cases the calculations diverge before the thermal wave reaches a fully developed condition.

TEMPERATURE PROFILES

Chemical Reactions

The combustion of the carbonaceous residue occurs according to the reaction

$$C + O_2 \rightarrow CO_2, \tag{3}$$

which is highly exothermic, releasing $|\Delta H_1| = 7{,}839$ kcal (32,816 kJ) per Kg of carbon.

At high enough temperatures the carbon can react with the carbon dioxide produced by the carbonate decomposition or by the carbon combustion producing carbon monoxide,

$$C + CO_2 \rightarrow 2\,CO. \tag{4}$$

The reaction is endothermic, absorbing $|\Delta H_2| = 2{,}202$ kcal (9,219 kJ) per kg of carbon. We let b = the moles of carbon consumed per mole of oxygen reacting, so that $b - 1/b$ is the fraction of carbon reacting with carbon dioxide and $1/b$ is the fraction reacting with

oxygen. The combined heat effect of Reactions 3 and 4 gives the heat released per kg of carbon consumed: $|\Delta H_c| = (1/b)\,|\Delta H_1| - (b-1)/b\,|\Delta H_2|$.

The carbonates, mainly dolomite and calcite, decompose, releasing carbon dioxide:

$$\text{Dolomite: } MgCO_3 \rightarrow MgO + CO_2 \tag{5}$$

$$\text{Calcite: } 5CaCO_3 + 2SiO_2 \rightarrow 2Ca_2SiO_4 + CaO + 5CO_2 \tag{6}$$

The decomposition of the dolomite absorbs $|\Delta H_3| = 375$ kcal (1,570 kJ) per kg of $MgCO_3$ (3×10^6 J/kg CO_2). The decomposition of calcite absorbs $|\Delta H_4| = 301$ kcal (1,261 KJ) per kg of $CaCO_3$.

The stoichiometry and kinetics of the pyrolysis of kerogen differs with the provenance of the shale (Crowl and Hoenle, 1980; Burnham and Braun, 1983; Burnham et al., 1982; Campbell et al., 1978). We consider a Western shale and adopt the reaction scheme worked out by Braun (1981). The kerogen decomposes to give oil, a combustible gas, CO_2, H_2O, and a carbon residue. Part of the oil produced is in the gas phase $(oil)_g$ and part in the liquid phase $(oil)_l$.

$$\begin{aligned}&1 \text{ kg kerogen} \rightarrow 0.6585X(T) \text{ kg } (oil)_g\\ &+0.6585[1 - X(T)] \text{ kg } (oil)_l + 0.0817 \text{ kg combustible gas}\\ &+0.0390 \text{ kg } CO_2 + 0.0378 \text{ kg } H_2O\\ &+0.1830 \text{ kg C}\end{aligned} \tag{7}$$

This reaction is endothermic, $|\Delta H_5| = 79$ kcal (330 kJ) per kg of kerogen. The details of the process by which oil is evolved from the kerogen are not well known (Richardson et al., 1982; Wallman et al., 1981). According to Campbell et al. (1978) the fraction of the oil in the gas phase, $X(T)$, can be calculated by considering the distillation curve for the oil:

$$\begin{aligned}X(T) &= 0.38 + (T - 598)(0.0035)\\ &\quad \text{for } T \geq 490 \text{ K}\\ &= 1.00\\ &\quad \text{for } T \geq 773 \text{ K}\end{aligned} \tag{8}$$

If the liquid oil remains in a hot zone for a sufficient period of time it cokes, yielding a carbonaceous residue and a gaseous product according to the scheme,

$$\begin{aligned}&0.7038 \text{ kg C/kg oil} + 0.2531 \text{ kg comb. gas/kg oil}\\ &\quad + 0.0431 \text{ kg } H_2O\text{/kg oil}\end{aligned}$$

$$(Oil)_l \xrightarrow{K_7} \qquad (Oil)_l \xrightarrow{K_v} (Oil)_g, \tag{9}$$

involving two parallel reactions, coking and vaporization, with rate constants K_7 and K_v respectively. The thermal effect of these reactions is neglected.

The gas temperature is much higher than the solid temperature at the same position in the bed, so the oil vapor $(oil)_g$ is subjected to thermal cracking (Burnham, 1981; Burnham et al., 1980; Bissel et al., 1983):

$$1 \text{ kg } (oil)_g \rightarrow 0.31 \text{ kg C} + 0.69 \text{ kg combustible gas} \tag{10}$$

The thermal effect of this reaction is not well known but can be ignored (Braun, 1981).

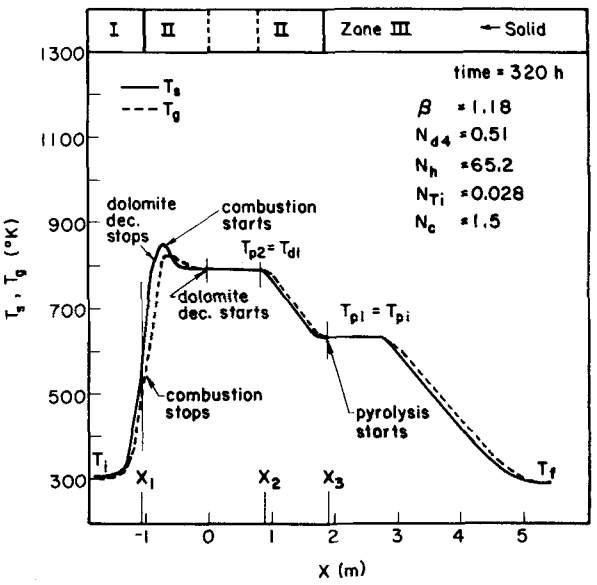

Figure 1. Fully developed temperature profile for the case of $\beta > 1$, $N_{d4} < 1$.

In the presence of oxygen the oil and gas produced will burn:

$$\begin{aligned}&1 \text{ kg oil} + 2.04 \text{ kg } O_2 \rightarrow 3 \text{ kg } CO_2 + H_2O\\ &1 \text{ kg gas} + 3.00 \text{ kg } O_2 \rightarrow 2.7 \text{ kg } CO_2 + H_2O\end{aligned} \tag{11}$$

These reactions are very exothermic, $|\Delta H_9| = 5{,}130$ kcal (21,480 kJ) per kg of oil, and $|\Delta H_{10}| = 6{,}606$ kcal (27,660 kJ) per kg of gas.

Characteristics of the Thermal Waves

Figures 1–4 show the different types of thermal waves calculated for combustion retorting. In order to facilitate the discussion of these curves we identify three types of zones: zone I represents the region where the incoming gas is heated up by contacting the hot burned shale; zone II, the regions where chemical reactions are occurring; zone III, the region where hot gases emerging from the reaction zones heat up the raw shale. No reactions occur in zones I or III, either because the temperature is too low or because reacting species are depleted.

Figures 1–3 consider the case of $\beta > 1$ for which the combustion occurs in the back part of the thermal wave. As already shown in HH-1, zone I is at a steady state condition in a coordinate system moving with the combustion front and zone III is an unsteady state region which becomes more diffuse as time proceeds.

The dolomite starts to decompose at a lower temperature than calcite. Figure 1 represents a situation in which the bed temperature is never high enough for calcite decomposition to occur. In this case $N_{d4} < 1$, where

$$N_{d4} = T_{ad}/T_{dl}. \tag{12}$$

Here, T_{ad} is the adiabatic temperature of the bed if the dolomite is decomposed,

$$T_{ad} = T_i + \frac{|\Delta H_c|\chi_s(1 - \psi_s) - |\Delta H_3|\chi_d}{C_s(\beta - 1)}, \tag{13}$$

and T_{dl}, is the temperature at which the dolomite starts decomposing. From the kinetic expression for the dolomite decomposition reaction, Eq. 44,

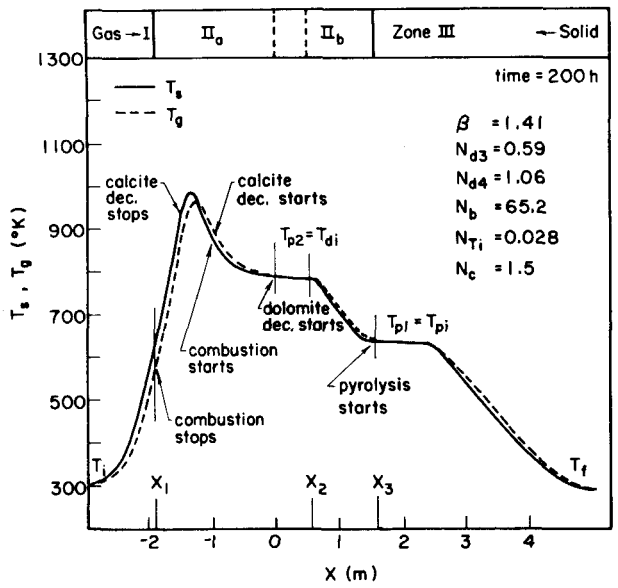

Figure 2. Fully developed temperature profile for the case of $\beta > 1$, $N_{d4} > 1$, $N_{d3} < 1$.

$$T_{di} = \frac{E_3}{-R \ln\left[\dfrac{d\delta/dx\, V}{\delta A_3}\right]} \qquad (14)$$

$$\frac{d\delta}{dx} \to 0 \qquad \delta = 1$$

For the situation in Figure 2 all the dolomite and part of the calcite decompose. In this case, $N_{d3} < 1$ and $N_{d4} > 1$, where N_{d4} is defined by Eq. 12 and N_{d3} by Eq. 2, with

$$T_{adc} = T_i + \frac{|\Delta H_c|\chi_s(1-\psi_s) - |\Delta H_3|\chi_d - |\Delta H_4|\chi_c}{C_s(\beta - 1)} \qquad (15)$$

For Figure 3, $N_{d3} > 1$ so all of the calcite and dolomite decomposes.

It is noted that in the cases depicted in Figures 1–3 the region where pyrolysis occurs is far downstream from the combustion

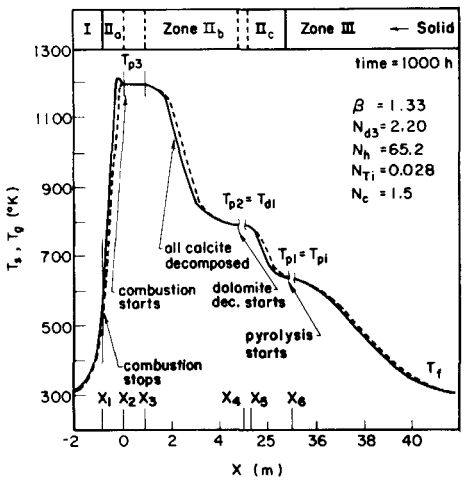

Figure 3. Fully developed temperature profile for the case of $\beta > 1$, $N_{d3} > 1$.

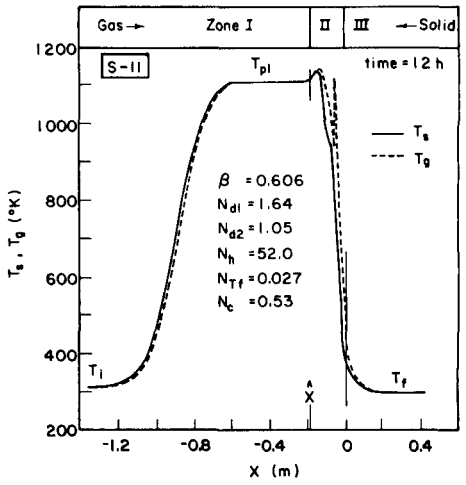

Figure 4. Fully developed temperature profile for run S-11 (Campbell, 1981).

region. The net heat of reaction is stored in plateau regions which increase in size as time proceeds. One of these is at the temperature at which the decomposition of dolomite is initiated, T_{di}, Eq. 14. Another is the temperature at which the pyrolysis reaction begins, T_{pi}. From the kinetic equation for this reaction, Eq. 46, the following relation for T_{pi} is obtained:

$$T_{pi} = \frac{E_5}{-R \ln\left[\dfrac{d\kappa/dx\, V_P}{\kappa A_5}\right]} \qquad (16)$$

$$\frac{d\kappa}{dx} \to 0 \qquad \kappa = 1,$$

where κ is the fraction of the initial kerogen remaining and V_p is the velocity of the pyrolysis front given by Eq. 22.

The case of $\beta < 1$, depicted in Figure 4, has the combustion occurring at the front of the wave and, in the back, a solid cooling which becomes more diffuse as time proceeds. All of the reactions occur in a single zone II which moves with velocity V given by Eq. 17. This reaction zone is separated from zone I by a plateau region which increases in length with increasing time.

Front velocities

As already pointed out in HH-1 and -2, the thermal waves shown in Figures 1–5 can be interpreted by considering the velocities of different thermal and reaction fronts.

The velocity of the combustion wave is obtained from a mass balance between the oxygen and the carbon:

$$V = \frac{3bN_o\dot{m}_g(1-\eta_s)}{8\rho_s\chi_s A(1-\epsilon)(1-\psi_s)} \qquad (17)$$

The velocity of a pure thermal wave is given by a heat balance:

$$V_{us} = \frac{\dot{m}_g C_g}{\rho_s C_s A(1-\epsilon)} \qquad (18)$$

From Eq. 1 it is seen that

$$\beta = V_{us}/V \qquad (19)$$

For $\beta > 1$, $V_{us} > V$ so the thermal wave (zone III in Figures 1–3) moves ahead of the combustion wave. For $\beta < 1$, $V_{us} < V$ so the thermal wave (zone I in Figure 4) falls behind the combustion wave.

In HH-2 we show how thermal fronts can be associated with the endothermic reactions. From overall heat balances the following velocities are calculated for each of these fronts:

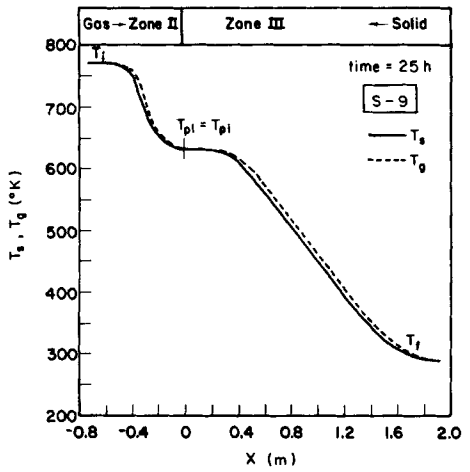

Figure 5. Fully developed temperature profile for run S-9 (Campbell, 1981).

Dolomite decomposition:

$$V_d = \frac{\dot{m}_g C_g}{A\rho_s C_s(1-\epsilon)} \frac{1}{1 + \dfrac{|\Delta H_3|\chi_d + |\Delta H_2|\chi_s(1-\psi_s)}{C_s(T_m - T_{di})}} \tag{20}$$

Calcite decomposition:

$$V_c = \frac{\dot{m}_g C_g}{A\rho_s C_s(1-\epsilon)} \frac{1}{1 + \dfrac{|\Delta H_4|\chi_c + |\Delta H_2|\chi_s(1-\psi_s)}{C_s(T_m - T_{ci})}} \tag{21}$$

Kerogen decomposition:

$$V_p = \frac{\dot{m}_g C_g}{A\rho_s C_s(1-\epsilon)} \frac{1}{1 + \dfrac{|\Delta H_5|\chi_k}{C_s(T_m - T_{pi})}} \tag{22}$$

In these equations ψ_s is the fraction of carbon remaining after the CO_2—C reaction takes place, T_m is the temperature of the gas entering the reaction front, and T_{pi}, T_{di}, T_{ci} are the temperatures at which kerogen, dolomite, or calcite start decomposing.

Since the heat needed to decompose the dolomite is larger than the heat needed to decompose the calcite, the calcite front moves faster than the dolomite front ($V_c \geq V_d$). However it is not possible for these two fronts to separate. The dolomite decomposition reaction has a lower activation energy and is initiated at a lower temperature at the front of the thermal wave. Consequently, the calcite front can overtake, but not pass, the dolomite front. When calcite decomposition is occurring, the dolomite and calcite decompositions are combined in a single front moving at the velocity

$$V_{cd} = \frac{\dot{m}_g C_g}{A\rho_s C_s(1-\epsilon)} \times \frac{1}{1 + \dfrac{|\Delta H_3|\chi_d + |\Delta H_4|\chi_c + |\Delta H_2|\chi_s(1-\psi_s)}{C_s(T_m - T_{di})}} \tag{23}$$

In the case $\beta > 1$, $N_{d3} < 1$ the maximum temperature of the bed T_m is not very high, causing $V_{cd} < V$. However, the combustion front can never move ahead of the decomposition front because, being associated with a temperature rise, it causes the carbonates to decompose. Therefore the two fronts move together at a velocity V, Eq. 17.

For the case $\beta > 1$, $N_{d3} > 1$, in which all the carbonate decompose, $V_{cd} > V$ so the carbonate decomposition front moves ahead of the combustion region. The plateau, T_{p3}, that develops increases in size at a rate $V_{cd} - V$.

In all the cases of $\beta > 1$ (Figures 1–3) the pyrolysis front has a velocity, V_p, greater than the other reaction fronts. Consequently it moves ahead of them, creating a plateau, $T_{p2} = T_{di}$, of increasing length. The thermal wave velocity V_{us}, is greater than V_p so it moves ahead of the pyrolysis front, creating a plateau, $T_{p1} = T_{pi}$, which increases in size with velocity $V_{us} - V_p$.

In the case $\beta < 1$ (Figure 4) the combustion front moves faster than all the other reaction fronts. Consequently, it overtakes them and all the reactions occur in a single zone II which moves at velocity V, given by Eq. 17. This reaction zone is separated from zone I by a plateau, T_{p1}, whose length increases with time at a rate $V - V_{us}$.

CONVERSIONS

Oil Yield

In the case $\beta > 1$ (Figures 1–3) the gas emerging from the decomposition zone at $T_{p2} = T_{di}$ causes the pyrolysis of the kerogen. Since the gas contains no oxygen, the pyrolysis can be viewed as the same as would be obtained by thermally retorting a bed of shale particles by a hot inert gas at temperature T_{di} (depicted in Figure 5). The main causes of oil loss in thermal retorting are the coking and cracking of the oil.

Coking is the degradation of the oil while it is in the liquid phase. Its severity depends on the time it takes the oil to vaporize. This in turn is proportional to the heating rate of the solid. A dimensionless group which is inversely proportional to the heating rate of the solid is used to account for the severity of coking:

$$N_c = \left(\frac{A_7\rho_g\epsilon C_g\, 10^{-6}}{h_{gs}a_p}\right)^{1/2} \frac{\dot{m}_g}{A\rho_s V_p(1-\epsilon)} \tag{24}$$

Cracking, which is the thermal degradation of the oil in the gas phase, varies inversely with the rate at which the oil vapor is cooled.

In the case $\beta < 1$ (Figure 4) the gas is not depleted of its oxygen when it enters the pyrolysis zone. This oxygen bypassing the combustion zone is consumed by burning the combustible gases, the oil vapors, and the oil liquids present in the pyrolysis region. This is the cause of the secondary peak in the gas temperature shown in zone II of Figure 4. This oil combustion, which is directly proportional to η_s, is the principle cause of oil loss. The coking of the oil in this case is less severe than in the case $\beta > 1$ because of the higher heating rates. Even though the gas reaches high temperatures, oil cracking is negligible because of the rapid cooling of the gas.

Carbonate Decomposition

The degree of carbonate decomposition is represented by the dimensionless groups N_{di}. The pertinent groups for $\beta > 1$ are N_{d3}, defined by Eq. 2 and N_{d4}, defined by Eq. 12.

In the case $\beta > 1$, $N_{d3} > 1$ all the dolomite and calcite are decomposed ($\delta_s = 0$, $\gamma_s = 0$). In the case $\beta > 1$, $N_{d3} > 1$ all the dolomite, $\delta_s = 0$, and part of the calcite, $1 - \gamma_s$, decompose. The fraction of calcite remaining, γ_s, can be calculated from the following heat balance:

$$T_{di} = T_i + \frac{|\Delta H_c|\chi_s - |\Delta H_3|\chi_d - |\Delta H_4|\chi_c(1-\gamma_s)}{C_s(\beta - 1)} \tag{25}$$

For $\beta > 1$, $N_{d4} < 1$ none of the calcite, $\gamma_s = 1$, and a fraction of the dolomite, $1 - \delta_s$, decompose. The fraction of the dolomite remaining, δ_s, can be calculated from the heat balance equation,

$$T_{di} = T_i + \frac{|\Delta H_c|\chi_s - |\Delta H_3|\chi_d(1-\delta_s)}{C_s(\beta - 1)} \tag{26}$$

In the case $\beta < 1$ the heat needed to decompose the carbonates is provided by combustion of products of the kerogen decomposition (oil and gas), in addition to the combustion of carbon. The oxygen will burn oil products before they have time to coke or crack. Therefore, from Eqs. 7, 11, and 12 we calculate that the combustion of oil and gas produced from the decomposition of 1 kg kerogen will consume 1.59 kg of oxygen and release $|\Delta H_o| =$ 3,920 kcal (16,413 kJ). From an overall heat balance,

$$T_{ad} = T_f + \frac{|\Delta H_c|\chi_s + |\Delta H_o|\chi_\kappa\kappa_s - |\Delta H_3|\chi_d - |\Delta H_5|\chi_\kappa}{C_s(1-\beta)} \tag{27}$$

$$T_{adc} = T_f + \frac{|\Delta H_c|\chi_s + |\Delta H_o|\chi_\kappa\kappa_s - |\Delta H_3|\chi_d - |\Delta H_4|\chi_s - |\Delta H_5|\chi_\kappa}{C_s(1-\beta)} \tag{28}$$

with κ_s being the fraction of the kerogen that burns in an oxygen environment. The parameter κ_s is related to η_s through the stoichiometric relation,

$$\kappa_s = \frac{\dot{m}_g N_o \eta_s}{1.59\, A\rho_s\chi_\kappa(1-\epsilon)V}. \tag{29}$$

Carbonate decomposition for $\beta < 1$ is characterized by the dimensionless groups,

$$N_{d1} = T_{ad/Tdf}, \tag{30}$$

$$N_{d2} = T_{adc}/T_{cf}, \tag{31}$$

with T_{ad} and T_{adc} defined by Eqs. 27 and 28. The terms T_{df} and T_{cf} represent the temperatures at which the dolomite and calcite decompositions stop. From the kinetics of these reactions,

$$T_{df} = \frac{E_3}{-R\ln\left[\dfrac{d\delta/dx\ V}{\delta A_3}\right]} \tag{32}$$

$$\frac{d\delta}{dx} \to 0 \qquad \delta = \delta_s$$

and

$$T_{cf} = \frac{E_4}{-R\ln\left[\dfrac{d\gamma/dx\ V}{\gamma A_4}\right]} \tag{33}$$

$$\frac{d\gamma}{dx} \to 0 \qquad \gamma = \gamma_s$$

For $\beta < 1$ we can have complete decomposition of the dolomites ($N_{d2} > 1$), partial decomposition of the calcite and complete decomposition of the dolomite ($N_{d1} > 1$, $N_{d2} < 1$), or partial decomposition of the dolomite ($N_{d1} < 1$).

NUMERICAL CALCULATIONS

Heat Balance Equations

The heat balance equations for the gas and solid phase temperature profiles are as follows:

$$\rho_g\epsilon C_g\frac{\partial T_g}{\partial t} = h_{gs}\alpha_p(1-\epsilon)(T_s - T_g) - \frac{\dot{m}_g}{A}C_g\frac{\partial T_g}{\partial z}, \tag{34}$$

$$\rho_s(1-\epsilon)C_s\frac{\partial T_s}{\partial t} = -h_{gs}\alpha_p(1-\epsilon)(T_s - T_g) - (1-\epsilon)\rho_s\sum_i \Delta H_i\, r_i\chi_i, \tag{35}$$

where, h_{gs} is the heat transfer coefficient between the gas and the solid, r_i is the rate of disappearance of species by chemical reaction, ΔH_i is the heat effects associated with that reaction, and χ_i is the weight fraction of species i in the solid. For simplification, fluid properties have been assumed constant and dispersion has been neglected. These assumptions are discussed in a later section.

If it is assumed that the temperature profile is steady to an observer moving with a velocity, V, the partial differential equations, Eqs. 34 and 35, are converted to ordinary differential equations.

$$-\frac{\dot{m}_g}{A}C_g\frac{dT_g}{dx} + h_{gs}a_p(1-\epsilon)(T_s - T_g) = 0 \tag{36}$$

$$V\rho_s C_s(1-\epsilon)\frac{dT_s}{dx} - h_{gs}a_p(1-\epsilon)(T_s - T_g) - (1-\epsilon)\rho_s\sum_i \Delta H_i\, r_i\chi_i = 0 \tag{37}$$

Solution of Heat Balance Equations without Chemical Reaction ($r_i = 0$)

The temperature profiles in zones I and III in Figures 1–5 are obtained by solving Eqs. 34–37 for the case of $r_i = 0$. In HH-1 it is shown that for a given temperature wave, steady state temperature profiles cannot exist for both zones I and III. For $\beta < 1$, zone I is steady and zone III is unsteady; for $\beta > 1$ zone III is steady and zone I is unsteady.

The steady state profiles are described by the following equations:

$$T_g = P + S\exp(-\alpha x), \tag{38}$$

$$T_s = P + S\beta\exp(-\alpha x), \tag{39}$$

with

$$\alpha = (1-\beta)\frac{h_{gs}a_p(1-\epsilon)A}{\dot{m}_g C_g} \tag{40}$$

The parameters P and S are constants obtained by matching the temperature profiles in this zone with the temperature profiles in the adjacent reaction zone.

The unsteady state temperature profiles are obtained by solving Eqs. 34 and 35 numerically with $r_i = 0$. Details about these numerical solutions and their matching to the adjacent reaction zone are given in HH-1.

Reaction Kinetics

The reactions occurring in the solid are analyzed by assuming spherical particles, isothermal and homogeneous.

The rate of carbon combustion, Eq. 3, is calculated by the expression,

$$r_1 = \left(\frac{\partial\psi}{\partial t}\right)_{\text{comb.}} = \frac{-9\rho_g N_o}{8\chi_s\rho_s R_p}\,\frac{\eta}{\left(\dfrac{R_p(\psi^{-1/3}-1)}{D_e} + \dfrac{3\rho_g N_o\psi^{-2/3}}{8\chi_s\rho_s R_p A_1\exp(-E_1/RT_s)} + \dfrac{1}{K_g}\right)}, \tag{41}$$

TABLE 1. VALUES OF KINETIC PARAMETERS FOR OUR MODEL

Reaction No.	A h^{-1}	E kcal/kmol	(kJ/kmol)	Reference
1	$9.01\ 10^{8}$	22,020	(92,190)	Sohn & Kim, 1980
2	$2.05\ 10^{8}$	40,260	(168,600)	Braun, 1981
3	$6.12\ 10^{13}$	57,800	(242,000)	Campbell, 1978
4	$3.45\ 10^{14}$	72,100	(301,860)	Braun, 1981
5	$1.01\ 10^{17}$	52,400	(219,400)	Campbell et al., 1978
7	$1.12\ 10^{11}$	35,000	(146,550)	Campbell et al., 1978
8	$1.73\ 10^{12}$	38,500	(161,200)	Burnham, 1981

K_g = 60 m/h (DeAcetis, 1960)
ρ_g = 0.44 kg/m^3 (Perry, 1969)
C_g = 0.523 kcal/kg·K (2.2 kJ/kg·K) (Perry, 1969)
C_s = 0.305 kcal/kg·K (1.27 kJ/kg·K)

derived by assuming that the chemical rate is first-order in oxygen and carbon and that the combustion occurs on the surface of a shrinking core. The development of this equation is explained in HH-1 and -2. The effective diffusion coefficient for the diffusion of the oxygen through the porous burned solid can be estimated by the following expression (Mallon and Braun, 1976):

$$D_e = 1.48\ 10^{-5}\ \chi_\kappa^2 T_s^{1.7}, \tag{42}$$

where D_e is expressed in m^2/h. The oxygen diffusion inside the particle is hindered by the generation of the CO_2 from the carbonate decomposition. Attempts to account for this effect using a model proposed by Sohn and Braun (1982) are not in good agreement with the experimental results, as discussed in HH-2.

We use a rate expression for carbon gasification by carbon dioxide, Eq. 2, developed by Ergun (1956):

$$r_2 = \left(\frac{\partial \psi}{\partial t}\right)_{\text{gas.}} = -\frac{\psi A_2 \exp(-E_2/RT_s)}{1 + \dfrac{\xi}{K_{\text{eq}}\theta}}, \tag{43}$$

where $K_{\text{eq}} = 4.15 \times 10^3 \exp(-11{,}400/T_s)$, ξ is the weight fraction of CO in the gas, and θ is the weight fraction of CO_2.

The dolomite and calcite decomposition reactions, Eqs. 5 and 6, are first-order with respect to the dolomite and calcite concentrations:

$$r_3 = \frac{\partial \delta}{\partial t} = -K_3\delta, \tag{44}$$

$$r_4 = \frac{\partial \gamma}{\partial t} = -K_4\gamma, \tag{45}$$

where δ and γ are the fractions of the dolomite and calcite remaining.

The kinetics of the kerogen decomposition, Eq. 7, depends on the origin of the oil shale (Burnham et al., 1982; Crowl and Hoenle, 1980). For a Western shale, the kinetics for the decomposition of the kerogen is first-order with respect to the kerogen concentration:

$$r_5 = \frac{\partial \kappa}{\partial t} = -K_5\kappa \tag{46}$$

The mechanisms for the evolution and degradation of the oil are not well understood; reaction schemes use empirical fits to data for the retorting of a particular shale (Campbell et al., 1978; Wallman et al., 1981; Richardson et al., 1982). An effort by Burnham and Braun (1983) to develop a theoretical model describing the decomposition of the kerogen and the evolution of the oil had a limited success. The model, which uses 67 first-order nonlinear ordinary differential equations, is much too complicated. Therefore, for ease of calculation we used a scheme tailored for the treatment of the modified in situ retorts for which oil yields of more than 100% Fisher assay are not obtained. In this scheme (Campbell et al., 1978), represented by Reaction 9, the liquid oil (λ_l) is consumed either by coking or by evaporation at a rate given by the following expressions:

$$r_{71} = \left(\frac{\partial \lambda_l}{\partial t}\right)_{\text{evap.}} = -K_v\lambda_l, \tag{47}$$

$$r_{72} = \left(\frac{\partial \lambda_l}{\partial t}\right)_{\text{coking}} = -K_7\lambda_l, \tag{48}$$

$$r_{73} = \left(\frac{\partial \lambda_l}{\partial t}\right)_{\text{cons.}} = r_{71} + r_{72}. \tag{49}$$

The rate of evaporation is proportional to the heating rate of the liquid, so the expression for K_v is as follows (Campbell et al., 1978):

$$K_v = 0.12\left|\frac{\partial T_s}{\partial t}\right|, \tag{50}$$

where K_v is expressed in (h^{-1}) and $|\partial T_s/\partial t|$ in (K/h). The cracking of the oil in the gas phase (Burnham et al., 1980; Burnham, 1981; Bissel et al., 1983) can be considered a first-order reaction with respect to the oil vapors concentration (λ_g).

$$r_8 = \left(\frac{\partial \lambda_g}{\partial t}\right)_{\text{crack.}} = -K_8\lambda_g. \tag{51}$$

The combustion rate of the oil and gas in the presence of oxygen is very fast, and therefore considered as instantaneous.

The values of the kinetic parameters for the chemical reactions are summarized in Table 1.

Steady State Mass Balance Equations

In a coordinate system moving with the velocity, V, of the reaction front, the mass balance equations change from partial differential equations to ordinary differential equations. The mass balance equations are as follows if Campbell's kinetics are used for the oil coking and if $\eta = 0$ and $\kappa = 0$ indicate the absence of oxygen and kerogen:

Kerogen:
$$\frac{d\kappa}{dx} = -\frac{r_5}{V} \tag{53}$$

Oil (liquid):
$$\frac{d\lambda_l}{dx} = \frac{0.6585[1 - X(T)]r_5}{V} - \frac{r_7}{V} \tag{54}$$

Oil (vapor):
$$\frac{d\lambda_g}{dx} = \frac{-\rho_s\chi_\kappa(1-\epsilon)A}{\dot{m}_g} \times [0.6585\,X(T)r_5 + r_{72}] + \frac{\epsilon\rho_g A}{\dot{m}_g} r_8 \tag{55}$$

Carbon:

$$\frac{d\psi}{dx} = \frac{0.183\chi_\kappa r_5}{\chi_s V} + \frac{0.7038\chi_\kappa r_{71}}{\chi_s V} + \frac{0.31\epsilon\rho_g r_8}{V\rho_s(1-\epsilon)\chi\kappa} - \frac{r_1 + r_2}{V} \quad (56)$$

Dolomite:

$$\frac{d\delta}{dx} = -\frac{r_3}{V} \quad (57)$$

Calcite:

$$\frac{d\gamma}{dx} = -\frac{r_4}{V} \quad (58)$$

Oxygen:

$$\frac{d\eta}{dx} = -\frac{8A\chi_s\rho_s(1-\epsilon)}{3\dot{m}_g N_o} r_1 \quad (59)$$

Carbon Dioxide:

$$\frac{d\theta}{dx} = \frac{-44p_s(1-\epsilon)A}{\dot{m}_g}\left[\frac{r_3\chi_d}{84} + \frac{r_4\chi_c}{100} + \frac{(r_1 - r_2)\chi_s}{12}\right] \quad (60)$$

Carbon Monoxide:

$$\frac{d\xi}{dx} = \frac{-28\chi_s\rho_s A(1-\epsilon)}{6\dot{m}_g} r_2 \quad (61)$$

The overlapping of the combustion and pyrolysis zones brings the oxygen IN contact with the gas and the oil. The combustion reaction, being very fast, stops only if the combustible species or the oxygen are depleted. We assume that in the region where the oil is burned the combustion of the carbon stops ($r_1 = 0$). This is justified because of the low oxygen concentrations, the hindering of the oxygen diffusion by the products of the pyrolysis reaction, and the small length of the overlap. In the pyrolysis and oil burning zone $\lambda_l = \lambda_g = 0$, $\kappa, \psi, \delta, \gamma, \xi$ are obtained from Eqs. 53, and 56–58, and 61, and η, θ, from the following expressions

$$\frac{d\eta}{dx} = \frac{1.6\rho_s\chi_\kappa(1-\epsilon)A}{\dot{m}_g N_o} r_5 \quad (62)$$

$$\frac{d\theta}{dx} = \frac{-44\rho_s(1-\epsilon)A}{\dot{m}_g}\left[\frac{r_3\chi_d}{84} + \frac{r_4\chi_c}{100}\right] - \frac{2.26\rho_s(1-\epsilon)A\chi_\kappa r_5}{\dot{m}_g} \quad (63)$$

Thermal Retorting

In pure thermal retorting, depicted in Figure 5, a hot gas at a temperature T_i and a flow rate $\dot{m}_g$, is used to retort oil shale. At a fully developed stage the solid is heated up by the gas at T_{pt}, Eq. 16, in zone III. The pyrolysis reaction starts at this temperature and continues until the kerogen is depleted. The pyrolysis front moves at a velocity V_p given by Eq. 22. The temperature and composition profiles for the pyrolysis zone are obtained by solving Eqs. 36, 37, and 53–56 with V_p substituted for V and $r_1 = 0$, $r_2 = 0$. Because the temperature T_i is not high enough for the carbonates to decompose $r_3 = 0$, $r_4 = 0$. The boundary conditions used to solve this problem are as follows:

$x = 0$	$T_s = T_g = T_{pt}$, Eq. 14
	$\kappa = 1$
	$\psi = 0$
	$\lambda_l = 0$
	λ_g = guess
$x = -\infty$	$T_s = T_g = T_i$
	$\kappa = 0$
	$\psi = 0$
	$\lambda_l = 0$
	$\lambda_g = 0$

This simple boundary value problem is solved using a standard method for ordinary differential equations (Carnahan et al., 1976).

Combustion Retorting $\beta > 1$

As explained in HH-2, the case $\beta > 1$ (Figures 1–3) is characterized by a pyrolysis front that moves faster than the other fronts and separates from them. The pyrolysis zone may be pictured as occurring by thermal retorting with a hot inert gas ($\eta = 0$) at a temperature T_{di}. This zone has to match the other zones at its boundaries.

At the matching with the decomposition zone $T_{p1} = T_g = T_s = T_{di}$, Eq. 14, and $\psi = 1$. The calculation of the temperature profiles for the combustion and decomposition zones are described in HH-2. In order to satisfy the matching conditions between the different zones an iterative computation is used.

Combustion Retorting $\beta < 1$

In the case $\beta < 1$ (Figure 4) all the reactions are taking place in the same region. To obtain the temperature and composition profiles we solve Eqs. 36, 37 and 53–63 that account for the contact of the oil with the oxygen. The boundary conditions used are the following:

$x = \infty$	$T_s = T_g = T_f$
$x = 0$	$\eta = 0$
	$\psi = 0$
	$\kappa = 1$
	$\lambda_l = 0$
	λ_g = guess
	$\delta = 1$
	$\gamma = 1$
$x = \hat{x}$	$T_s = T_g = T_{p1}$ (from matching with zone I)
	$\eta = 1$
	$\psi = 0$
	$\kappa = 0$
	$\lambda_l = 0$
	$\lambda_g = 0$
	$\theta = 0$
	$\xi = 0$
	$r_3 = 0$: no more decomposition
	$r_4 = 0$:

The nonlinearity of the equations and the sensitivity of the computer computations to round off errors forced us to use double precision numerics and the method of Gear (1971) for the numerical integrations. By guessing the amount of oil coked and neglecting the cracking we can use the method described in HH-2 (Appendix 1) to solve for the temperature and composition profiles. An iterative process is used to calculate the amount of oil coked.

RESULTS

The calculated temperature and composition profiles are summarized in Figures 1–5 and in Tables 2–4.

Oil Yield

From our calculations it is seen that the yield losses due to the combustion of the oil for the case of $\beta < 1$ (Table 4) are of the same order as the yield losses due to the coking of the oil in the case of $\beta > 1$ (Tables 2 and 3). Cracking is found to be negligible in both cases.

TABLE 2. RESULTS FOR $\beta > 1$

	Fig. 1	Fig. 2	Fig. 3
Fisher Assay (L/t)	82	82	117
$\dot{m}_g/A$ (kg/h·m^2)	112	112	112
N_o	0.023	0.028	0.028
Carbonates (% wt)	36	36	11
R_p (m)	0.03	0.03	0.03
ϵ	0.311	0.311	0.311
β	1.18	1.41	1.33
N_{d3}	−0.42	0.59	2.20
N_{d4}	0.51	1.06	—
N_h	65.2	65.2	65.2
N_{Ti}	0.028	0.028	0.028
N_c	1.5	1.5	1.5
T_{p1} (K)	630	630	630
T_{p2} (K)	794	791	791
T_{p3} (K)	—	—	1197
V (m/h)	0.074	0.062	0.065
V_{cd} (m/h)	—	—	0.067
V_p (m/h)	0.1062	0.1059	0.100
ψ_s	0.50	0.20	0.018
b	1.06	1.15	1.95
δ_s	0.83	0.00	0.00
γ_s	1.00	0.87	0.00
Oil Yield (% Fish. ass.)	92.6	93.0	93.3

The parametrization of the problem shows the oil yield to be a function of η_s and N_c (Table 5).

Temperature and Composition Profile

In the case of $\beta > 1$, summarized in Table 2 and Figures 1–3, the presence of the kerogen adds one more front to the temperature profile. A comparison of the temperature and composition profiles for the combustion and decomposition zones with the calculations in HH-2 for a situation in which no kerogen is present (combustion of processed shale) does not show any difference. Therefore the analysis presented in HH-2 holds for this work.

In the case of $\beta < 1$ (Figure 4 and Table 4) the combustion of the oil releases a large amount of heat. This increases the temperature of the bed and decomposes all of the carbonates. The picture for the combustion of processed shale also is applicable to the case considered in this paper if the additional heat released by the oil combustion is taken into account.

The influence of the operating conditions on the composition profile is presented in Table 5. The dimensionless groups β, N_{d1}, N_{d2}, N_{d3}, N_{d4}, and N_c are given by Eqs. 1, 30, 31, 2, 12, and 24. The heat exchange group N_h is given by the following expressions:

$$N_h = \frac{h_{gs} a_p R_p^2}{\overline{D}_e C_g \rho_g}, \tag{64}$$

where $\overline{D}_e$ is the average value of the oxygen diffusion coefficient D_e. The groups N_{Tf} and N_{Ti} are related to the quench of the combustion reaction for $\beta < 1$ and $\beta > 1$ respectively and are defined by the following equations:

$$N_{Tf} = \frac{T_f R}{E_1} \tag{65}$$

$$N_{Ti} = \frac{T_i R}{E_1} \tag{66}$$

By using the heat and mass balances described in the section on thermal wave characteristics, Eqs. 12–16, one can calculate the main characteristics of the temperature and composition profiles if the values of η_s (or ψ_s) and b are known. We have developed in HH-2 a method to approximate these values. The presence of the kerogen in the bed complicates the calculations but alters the results only slightly. Therefore the method described in the section, "Design Considerations," in HH-2 can be used as a good first approximation.

TABLE 3. THERMAL RETORTING S-9*

$V = 0.095$ m/h
$T_{p1} = T_{pi} = 630$ K
$\psi_s = 0.0274$
$\delta_s = 1$
$\gamma_s = 1$
Oil Yield = 95.3% Fisher assay

* Experimental work, Lawrence Livermore Lab. (Campbell, 1981).

TABLE 4. RESULTS FOR RUN S-11*

	Experimental*	Calculated	Braun's Model**
β	0.622	0.606	0.575
N_{d1}	—	1.64	—
N_{d2}	—	1.05	—
N_h	—	52.0	—
N_{Tf}	—	0.027	—
N_c	—	0.53	—
T_p (K)	1,229	1,080	1,123
V (m/h)	0.110	0.113	0.119
$\hat{x}$ (m)	—	0.19	0.21
ψ_s	~0.00	0.00	0.00
b	1.08	1.04	1.07
δ_s	~0.00	0.00	0.00
γ_s	~0.00	0.00	0.00
Oil yield (% Fish. Ass.)	92	91	93
N_2 (% vol)	59.9	58	57
O_2 (% vol)	0.6	0.00	0.00
Combustiles (% vol)	7	5	7.7
CO_2	32.5	37	35.3

* Experimental work, Lawrence Livermore Lab. (Campbell, 1981).
** Braun (1981).

DISCUSSION

Comparison with Experimental Results

Since the time required to achieve the fully developed regime for the case of $\beta > 1$ (Figures 1–3) is very large, no experimental results are available, because the length of retort would be inconvenient for laboratory studies.

For the case of $\beta < 1$ (Figure 4) we have calculated the temperature and composition profiles corresponding to experiment S-11 performed at the Lawrence Livermore Laboratory (Campbell, 1981). In Table 4 we compare the results of our model to the experimental results and to the results obtained using Braun's (1981) model. As can be seen the accuracy of our model is very satisfactory. We also find good agreement between the temperature profiles calculated from our model (Figure 4) and the temperature profile calculated from Braun's model (Figure 6).

Discussion of the Assumptions

Nonuniformities in the combustion front and mixing in the gas

TABLE 5. INFLUENCE OF DIMENSIONLESS GROUPS ON COMPOSITION PROFILES

	β	N_h	N_{Tf}	N_{Tt}	N_{d1}	N_{d2}	N_{d3}	N_{d4}	N_c
Oil Yield	X	X	X	—	—	X	—	—	X
Oil Coking	—	—	—	—	—	—	—	—	X
η_s (oil burned)	X	X	X	—	—	X	—	—	—
ψ_s	X	X	—	X	—	—	X	—	—
b	X	—	—	—	—	X	X	—	—
δ_s	X	—	—	—	X	X	X	X	—
γ_s	X	—	—	—	X	X	X	X	—

phase will cause the temperature and composition profiles to be more diffuse than what we calculate. The same effect will also be caused by the increase of the gas flow rate because of gas generation from the decomposition of the solid (carbonates and kerogen). This spreading of the profiles will cause adjacent zones to overlap. In the case of $\beta < 1$ the increase in the overlapping of the combustion and pyrolysis zones will cause a significant amount of the oil to be burned since large portions of unretorted shale will be surrounded by the combustion front (Bickel, 1983). In the case of $\beta > 1$ this mixing has a small effect on the oil yield because the combustion and pyrolysis fronts are separated by a plateau region. This suggests that in the real situation the case of $\beta > 1$ will give better yields than the case of $\beta < 1$.

The oil vapor produced in the pyrolysis zone is carried to a region containing cold shale, where it condenses and flows down the bed as a liquid. A thin film of the liquid remains on the surface of the particles and is evaporated when the temperature of the particle rises. The heating of the oil to its vaporization temperature will cause coking. This coking is proportional to the heating rate of the oil. Modeling this coking is difficult because of the multicomponent structure of the oil and our ignorance of the heat of condensation. In the case of $\beta > 1$ the diffuse heating front will cause more oil losses than in the case of $\beta < 1$. These losses, assumed to be small, can be decreased by increasing the gas flow rate.

The nonuniformity in the particle sizes causes a nonuniformity in the combustion front. Therefore the bigger particles can be surrounded by oxygen before they have time to be retorted. In the case of $\beta > 1$ the absence of oxygen during the pyrolysis reaction hinders the combustion of the oil in the big particles.

All the above considerations lead us to conclude that $\beta > 1$, $N_{d3} > 1$ are the optimum conditions for the process.

OPERATING RECOMMENDATIONS

The calculations presented here support the suggestion in HH-2 that the best operating conditions to maximize the oil yield are $\beta > 1$, $N_{d3} > 1$. An analysis of these two groups shows that to achieve the conditions $\beta > 1$, $N_{d3} > 1$, one must use small ratios of the oxygen concentrations to the fuel (carbon) concentration. This condition is easy to satisfy in the case of an Eastern shale where the carbon residue is very high. In the case of a lean Western shale the small amount of the carbon requires a very low oxygen concentration in the gas. However, if this oxygen concentration drops below a certain level no combustion is possible. In this case, adding a fuel gas (which could be recycled exit gas) will increase the fuel concentration. The fuel in recycle gas will have the same effect as the carbon in the solid.

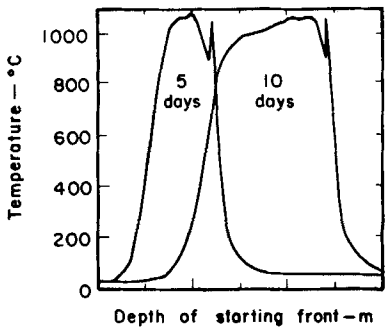

Figure 6. Gas phase temperature profiles for S-11 (Braun, 1979).

In order to minimize the ignition time and the associated oil losses we suggest the use of a special ignition process by which an inert gas at a temperature T_{di} is initially passed through the bed. This causes the kerogen to decompose and the pyrolysis front to move a certain distance into the bed, leaving behind a bed of pyrolyzed shale. This bed can then be ignited by using a cold gas feed containing oxygen.

In the recent experiments by Occidental on modified in situ retorting, the exposure of the roof to hot gases for large periods of time resulted in its collapse (Bickel, 1983). This collapse imposes an increase in the required overburden depth, and therefore in the separation needed between consecutive vertical retorts. This limitation is very critical for in situ retorting because it restricts the amount of shale that will be processed. This is a factor penalizing in situ retorting compared to aboveground retorting. In the case of $\beta > 1$, where all the known retorts have been operating, the very diffuse thermal front in zone I could cause a prolonged heating of the roof. In the case of $\beta > 1$, zone I has a very stiff steady state temperature profile. The absence of backward diffusion of heat could prevent prolonged heating of the roof.

CONCLUDING REMARKS

We have developed a steady state model for the combustion retorting of shale oil. The physical understanding of the process allows us to propose an operating strategy to optimize the oil yield.

To our knowledge all the experimental results for the fully developed regime are in the region of $\beta < 1$. We present a number of reasons why operation with $\beta > 1$ appears more advantageous.

ACKNOWLEDGMENT

The authors gratefully acknowledge support for this work received from the Shell Companies Foundation.

NOTATION

A_i = preexponential factor in the rate equation for reaction i
A = area of the bed section
a_p = ratio of the particle area to its volume

b = moles of carbon consumed per mole of oxygen
C_g = heat capacity of the gas
C_s = heat capacity of the solid
D_e = effective diffusion coefficient of oxygen through the burned shale
$\overline{D}_e$ = average value of D_s
E_i = activation energy for reaction i
h_{gs} = overall gas-solid heat transfer coefficient
i = 1 for $C + O_2 \rightarrow CO_2$
2 for $C + CO_2 \rightarrow 2CO$
3 for dolomite decomposition
4 for calcite decomposition
5 for kerogen decomposition
7 for oil coking
8 for oil cracking
9 for oil combustion
10 for gas combustion
K_g = mass transfer coefficient through the gas film surrounding the particle
K_i = rate constant for reaction i
K_v = rate of oil vaporisation
$\dot{m}_g$ = mass flux of the gas
N_o = weight fraction of the oxygen in the entry gas
R = universal gas constant
R_p = particle radius
r_i = rate of reaction i
T_{cf} = temperature at which calcite stops decomposing
T_{ci} = temperature at which calcite starts decomposing
T_{df} = temperature at which dolomite stops decomposing
T_{di} = temperature at which dolomite starts decomposing
T_f = initial temperature of the bed
T_{ad} = $T_f + \dfrac{|\Delta H_c|\chi_s + |\Delta H_o|\chi_\kappa\kappa_s - |\Delta H_3|\chi_d - |\Delta H_5|\chi_\kappa}{C_s(1-\beta)}$ for $\beta < 1$

= $T_i + \dfrac{|\Delta H_c|\chi_s(1-\psi_s) - |\Delta H_3|\chi_d}{C_s(\beta-1)}$ for $\beta > 1$

T_{adc} = $T_f + \dfrac{|\Delta H_c|\chi_s + |\Delta H_o|\chi_\kappa\kappa_s - |\Delta H_3|\chi_d - |\Delta H_4|\chi_c - |\Delta H_5|\chi_\kappa}{C_s(1-\beta)}$ for $\beta < 1$

= $T_i + \dfrac{|\Delta H_c|\chi_s(1-\psi_s) - |\Delta H_3|\chi_d - |\Delta H_4|\chi_c}{C_s(\beta-1)}$ for $\beta > 1$

T_g = gas temperature
T_i = gas temperature at entry section
T_m = maximum temperature
T_{pi} = temperature at which kerogen starts decomposing
T_{p1}, T_{p2}, T_{p3} = plateau temperatures
T_s = solid temperature
t = time
V = combustion front velocity
V_c = calcite decomposition front velocity
V_{cd} = carbonate decomposition front velocity
V_d = dolomite decomposition front velocity
V_p = pyrolysis front velocity
V_{us} = unsteady state heating zone velocity
x = length of the bed
$\hat{x}$ = length of the reaction zone
$X(T)$ = fraction of the oil in the gas phase at T
z = distance from the entry of the bed
χ_κ = weight fraction of kerogen in the raw shale
χ_i = weight fraction of the species i in the raw shale
ψ = fraction of carbon remaining
ψ_s = fraction of carbon remaining unburned at the end of the retort

Greek Letters

α = $(1-\beta)\dfrac{h_{gs}a_p(1-\epsilon)A}{\dot{m}_g C_g}$
β = ratio of heat capacity rates = $\dfrac{\dot{m}_g C_g}{VC_s(1-\epsilon)A\rho_s}$
γ = fraction of calcite remaining
γ_s = fraction of calcite remaining at the end of the operation
δ = fraction of dolomite remaining
δ_s = fraction of dolomite remaining at the end of the operation
$|\Delta H_c|$ = $|b\Delta H_1 + (b-1)\Delta H_2|/b$
$|\Delta H_o|$ = heat of kerogen combustion
$|\Delta H_i|$ = heat of reaction i
ϵ = void fraction
η = fraction of oxygen remaining
η_s = fraction of oxygen consumed by the oil and gas combustion
θ = weight fraction of CO_2 in the gas
θ_s = weight fraction of CO_2 in the exit gas
κ = fraction of kerogen remaining
κ_s = fraction of kerogen burned
$(\lambda)_l$ = fraction of the oil in the liquid phase
$(\lambda)_g$ = weight fraction of oil vapors in the gas
ξ = weight fraction of CO in the gas
ξ_s = weight fraction of CO in the exit gas
ρ_g = density of the gas
ρ_s = density of the solid
χ_c = weight fraction of calcite in the raw shale
χ_d = weight fraction of dolomite in the raw shale
χ_s = weight fraction of carbon in the process shale

Dimensionless Parameters

N_c = $\sqrt{\dfrac{A_7\rho_g\epsilon C_g 10^{-6}}{h_{gs}a_p}}\dfrac{\dot{m}_g}{A\rho_s V_p(1-\epsilon)}$
N_{d1} = $\dfrac{T_{ad}}{T_{df}}$
N_{d2} = $\dfrac{T_{adc}}{T_{cf}}$
N_{d3} = $\dfrac{T_{adc}}{T_{di}}$
N_{d4} = $\dfrac{T_{ad}}{T_{di}}$
N_h = $\dfrac{h_{gs}a_p R_p^2}{D_e C_g \rho_g}$
N_{Tf} = $\dfrac{T_f R}{E_1}$
N_{Ti} = $\dfrac{T_i R}{E_1}$

LITERATURE CITED

Ahmad, A., et al., "A Mathematical Model for *In Situ* Oil Shale Retorting,"

1st Int. Conf. on Math. Modeling, Univ. of Missouri, Rolla, MO (Aug., 1977).
Baer, A. D., and C. A. Dahl, "A Simple Semisteady-State Model of the Combustion Retort, *In Situ*, 4(1), 79 (1980).
Bickel, T., "Analysis of Occidental Vertical Modified in situ Retorts 7 and 8," Proc. 16th Oil Shale Symp., Colorado Sch. of Mines, Golden, CO (Apr., 1983).
Bissell, E. R., A. K. Burnham, and R. L. Braun, "Shale Oil Cracking Kinetics and Diagnostics," UCRL-89976, Lawrence Livermore Laboratory, Livermore, CA (1983).
Braun, R. L., "Results of Computer Simulation of In Situ Oil Shale Retorting," *In Situ*, 3(3), 173 (1979).
——, "Mathematical Modeling of Modified In Situ and Aboveground Oil Shale Retorting," URCL-53119, Lawrence Livermore Laboratory, Livermore, CA (1981).
Burnham, A. K., et al., "Shale Oil Cracking. 2: Effect on Oil Composition," UCID-18763, Lawrence Livermore Laboratory, Livermore, CA (1980).
Burnham, A. K., and R. L. Braun, "General Model of Oil Shale Pyrolysis," UCRL-89805, Lawrence Livermore Laboratory, Livermore, CA (1983).
Burnham, A. K., J. F. Richardson, and T. T. Corbun, "Pyrolysis Kinetics for Western and Eastern Oil Shale," UCRL-87587, Lawrence Livermore Laboratory, Livermore, CA (1982).
Burnham, A. K., "Oil Shale, Tar Sands, and Related Materials," *ACS Symp. Ser.*, **163**, 39, Amer. Chem. Soc., Washington, DC (1981).
Campbell, J. H., G. H. Koskinas, and N. D. Stout, "Oil Shale Retorting: Effects of Particle Size and Heating Rate on Oil Evolution and Intraparticle Oil Degradation," *In situ*, **2**(1), 1 (1978).
Campbell, J. H., "Kinetics of Decomposition of Colorado Oil Shale. II: Carbonate Minerals," UCRL-52089 (Pt 2), Lawrence Livermore Laboratory, Livermore, CA (1978).
——, "Modified In Situ Retorting: Results from LLNL Pilot Retorting Experiments, UCRL-52168, Lawrence Livermore Laboratory, Livermore, CA (1981).
Carnahan, B., H. A. Luther, and J. O. Wilkes, *Applied Numerical Methods*, 407, John Wiley and Sons, New York (1976).
Crowl, D. A., and W. F. Hoenle, "The Stoichiometry of the Pyrolysis of Michigan Oil Shale," *In Situ*, 4(4), 371 (1980).
DeAcetis, J., and C. Thodos, "Mass and Heat Transfer in Flow of Gases Through Spherical Packings," *Ind. Eng. Chem.*, **52**, 1,003 (1960).
Dockter, L., and T. F. Turner, "Combustion Rates for Oil Shale Carbonaceous Residue," *In Situ*, **2**(3), 197 (1978).
Ergun, S., "Kinetics of the Reaction of Carbon Dioxide with Carbon," *J. Phys. Chem.*, **60**, 480 (1956).
Fausset, D. W., "A Mathematical Model of an Oil Shale Retort," *Colorado School of Mines Qtly.*, **70**(3), 273 (1975).
Gear, C. W., *Numerical Initial Value Problems in Ordinary Differential Equations*, Prentice-Hall, Englewood Cliffs, NJ (1971).
Hiskakis, M., and T. J. Hanratty, "Combustion of Carbon Residue from Oil Shale Retorting," *AIChE J.*, **29**(3), 451 (1983).
Hiskakis, M., and T. J. Hanratty, "Fully Developed Temperature Waves in a Bed of Processed Shale," *AIChE J.*, **31** (1985).
Mallon, R. C., and R. L. Braun, "Reactivity of Oil Shale Carbonaceous Residue with Oxygen and Carbon Dioxide," *Colorado School of Mines Qtly.*, **71**(4), 309 (1976).
Nuttal, H. E., "Mathematical Modeling and Experimental Investigation of In Situ Oil Shale Retorting," 51st Ann. Meet. SPE-AIME, New Orleans (1976).
Perry and Chilton, *Chemical Engineers Handbook*, 5th Ed., McGraw-Hill, New York (1969).
Richardson, J. H., et al., "Fluidized-Bed Pyrolysis of Oil Shale: Oil Yield, Composition and Kinetics," UCID-19548, Lawrence Livermore Laboratory, Livermore, CA (1982).
Sohn, H. Y., and K. S. Kim, "Intrinsic Kinetics of the Reaction between Oxygen and Carbonaceous Residue in Retorted Oil Shale," *Ind. Eng. Chem. Proc. Des. Dev.*, **19**(4), 550 (1980).
Sohn, H. Y., and R. L. Braun, "The Effect of Internally-Generated Bulk Flow on the Rates of Gas-Solid Reactions. 1: Development of an Approximate Solution, UCRL-87976, Lawrence Livermore Laboratory, Livermore, CA (1982).
Tyner, C. E., and P. J. Hommert, "Numerical Modeling of a True In Situ Oil Shale Retorting," SAND-78-1306, Sandia Laboratories, Albuquerque, NM, (1979).
Wallman, P. H., P. W. Tamm, and B. G. Spars, "Oil Shale, Tar Sands, and Related Materials," *ACS Symp. Ser.* **163**, 93, Amer. Chem. Soc., Washington, DC (1981).

Manuscript received Mar. 26, 1984; revision received Oct. 10 and accepted Oct. 15, 1984.